Effect of surface carrier concentration on valence subbands in Si(111) *p*-type inversion layers: Angle-resolved photoemission spectroscopy

Sakura Nishino Takeda,* Naoto Higashi, and Hiroshi Daimon
Faculty of Materials Science, Nara Institute of Science and Technology, Nara 630-0192, Japan

(Received 28 April 2010; published 29 July 2010)

We investigated the effect of surface carrier concentration on the quantum levels and the in-plane effective masses of the subbands in Si(111) *p*-type inversion layers. Two inversion layers with different surface carrier concentrations were made as a result of metallic surface structures. The subband dispersion was measured by angle-resolved photoelectron spectroscopy. The energy levels of the observed subbands at $k=0.0$ Å^{-1} partially agree with the results of the calculation using the triangular approximation. The effective masses are not significantly affected by the surface carrier concentration. The spatial extension of the subband wave functions is discussed.

DOI: 10.1103/PhysRevB.82.035318 PACS number(s): 73.21.Fg

The scale of the complementary metal-oxide-semiconductor field-effect transistor (CMOSFET) reaches the decananometer level today due to continuous scaling down. In such devices, the depth of the inversion layer (IL) under the gate electrode is a few nanometer. Due to the quantum confinement effect along the depth direction, the electronic states in IL form two-dimensional energy bands, called subbands. The subband structure is closely related to the properties of the electron transport from the source to the drain in CMOSFET. Thus, from a technological point of view, a strong demand exists for the determination of the subband structures in IL.

Investigation of the subband structure in IL has a long history which dates back to when the quantization in IL was first postulated[1] and proven.[2] Effective masses of the subbands were measured using Shubnikov-de-Haas (SdH) oscillation[2–6] and cyclotron resonance (CR).[7–13] The energy-level separations of the quantum levels were measured by intersubband optical-absorption,[14–18] inelastic-light-scattering,[19,20] and photoconductivity measurements.[21,22] Far-infrared light emission through the intrasubband transition was also investigated.[23] These experiments have stimulated intensive theoretical studies. Subband effective mass was calculated using the Hartree approximation[24–27] and compared with the experimental results by SdH and CR. Importance of the many-body effect on the subband structure such as effective mass and energy separation was pointed out.[28–34] The results of the early works are summarized in a comprehensive review.[35]

Recently, several groups have revisited the quantized electronic structure in Si IL (Refs. 36–43) to achieve faster CMOSFET performance speed. Although for this purpose detailed information such as effective masses in specific directions and energy separations at certain wave vectors is necessary, it has not been provided experimentally. For detailed information, a direct measurement of the dispersion structure of the Si valence subband is needed. We have recently shown that the dispersion structure of the Si valence subbands is detectable using angle-resolved photoelectron spectroscopy (ARPES) on a metal-adsorbed Si surface.[44] An atomic layer of indium on the Si(111) clean surface acts as a "built-in electrode" and induces band bending without applying external voltage [see Figs. 1(a) and 1(b)]. The dispersion structure of the Si subband in the IL induced by the built-in electrode was clearly detected by ARPES.

In this paper, we report valence-subband structures under two different surface carrier concentrations (n_s). The change in n_s was achieved by altering the adsorbate metal which acts as the built-in electrode. The dependences of the subband energy and effective mass on n_s were discussed in comparison to the available theoretical results. As the two different built-in electrodes, indium-covered Si(111)$\sqrt{7}\times\sqrt{3}$-In structure[45,46] and lead-covered Si(111)$\sqrt{3}\times\sqrt{3}$-SIC-Pb structure,[47–49] where SIC means "striped incommensurate," were chosen. Hereafter, we shall refer to IL induced by $\sqrt{7}\times\sqrt{3}$-In ($\sqrt{3}\times\sqrt{3}$-SIC-Pb) as IL(In) [IL(Pb)]. Both surface structures are formed with approximately one monolayer metal overlayer[46,48] and both have large density of states at the Fermi level, which induces strong upward band bending.[46,47]

All surface preparations and ARPES measurements were done in an ultrahigh-vacuum chamber. The surface of Si(111)

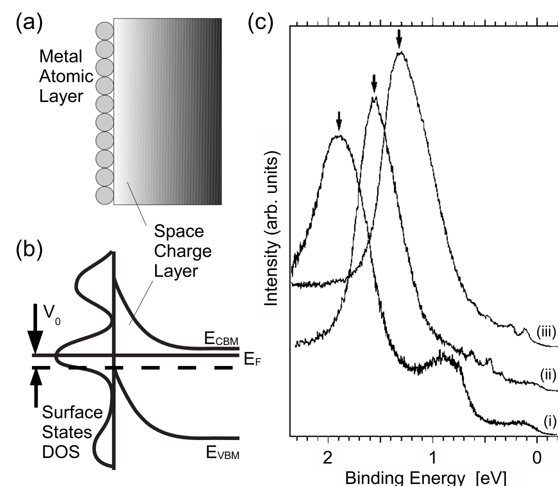

FIG. 1. The surface band bending induced by a metal atomic layer. (a) A schematic cross section of our sample and (b) the corresponding band bending. (c) ARPES spectra at $k=0.0$ Å^{-1} from (i) Si(111)7×7, (ii) $\sqrt{7}\times\sqrt{3}$-In, and (iii) $\sqrt{3}\times\sqrt{3}$-SIC-Pb surfaces. Arrows indicate Si 3*p* peaks.

 ©2010 The American Physical Society

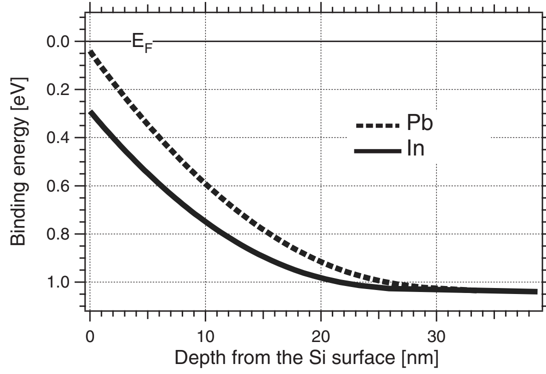

FIG. 2. Valence-band maximum E_{VBM} as a function of the depth.

substrates from the same wafer (p-type, impurity concentration of 1×10^{18} cm^{-3}) was cleaned by flash heating. Lead and indium were evaporated from alumina-coated tungsten baskets. During or after the deposition, substrate was annealed at 400–500 °C. The surface structure was monitored by reflection high-energy electron diffraction during deposition and annealing. After the $\sqrt{7}\times\sqrt{3}$-In or Si(111)$\sqrt{3}\times\sqrt{3}$-SIC-Pb structure was made, ARPES was done using the monochromatized He I light (21.2 eV) and a photoelectron analyzer (VG Scienta SES2002). The probing depth of ARPES in the present study was around 5 Å.[50] The sample was rotated around an in-plane rotational axis to detect photoelectrons over a wide range of emission angles. Sample temperature was at around 298 K during the ARPES measurement.

The band bendings induced by the surface structures were calculated using the following equation derived from the Poisson equation:[51]

$$z = L_D \int_{v_s}^{v} \frac{\mp dv}{\sqrt{2}[\cosh(u_b+v)/\cosh u_b - v \tanh u_b - 1]^{1/2}}.$$

Here z is the depth from the surface and L_D is the Debye length. L_D's for both ILs were 4.1 nm. v and u_b are expressed as $v=(E_b^i-E^i)/k_BT$ and $u_b=(E_F-E_b^i)/k_BT$. E_F, E^i, and E_b^i are the Fermi level, the middle of the band gap varying with z in the space-charge layer, and the middle of the band gap in the bulk. The lower limit of the integral v_s is expressed as $v_s=(E_b^i-E_s^i)/k_BT$. E_s^i is the middle of the band gap at the surface. In the case of Si(111)-7×7, the Fermi level is known to be pinned at 0.63 eV ($V_0^{7\times7}$) above the valence-band maximum (E_{VBM}) at the surface.[52] The differences between E_F and E_{VBM} at the surfaces of IL(In) (V_0^{In}) and IL(Pb) (V_0^{Pb}) are then obtained by adding the Si 3p (valence-band) peak shifts of each surface relative to that of 7×7 to $V_0^{7\times7}$. The energy shifts for $\sqrt{7}\times\sqrt{3}$-In and $\sqrt{3}\times\sqrt{3}$-SIC-Pb surfaces in ARPES spectra shown in Fig. 1(c) were measured to be −0.34 eV and −0.59 eV, respectively. Then, the V_0^{In} and V_0^{Pb} are obtained to be 0.29 eV and 0.04 eV, respectively. From these values, $E_b^i-E_s^i$, which determines v_s, is derived to be −0.41 eV for the 7×7, −0.75 eV for IL(In), and −1.00 eV for IL(Pb). The difference in the amount of the band bending between the IL(In) and IL(Pb) was obtained to be 0.25 eV from the Si 3p peak shift. The calculated band-bending shapes are shown in Fig. 2. The n_s was calculated to be 3.1×10^{12} cm^{-2} for IL(In) and 3.8×10^{12} cm^{-2} for IL(Pb). Surface photovoltage (SPV) effects were reported for ARPES measurement on semiconductor surfaces. This effect arises from the movement of photoinduced electron and holes toward opposite directions along the electric field gradient of band bending when it exists. By this effect, the amount of the original band bending tends to decrease. High photon flux density and low carrier recombination rate at low substrate temperature makes this effect significant. In the case of Si(111)7×7 at 100 K, the S_2 surface states peak was reported to shift by 0.7 eV by changing the photon flux.[53] At room temperature, however, the carrier recombination rate is high enough and no large SPV effect is expected.[53]

Dispersion structures of the valence subbands in both ILs measured by ARPES are shown in Figs. 3(a) and 3(b). The in-plane wave vector is in $[11\bar{2}]$ direction. The dispersion curves with light and heavy in-plane hole masses are visible in both ILs. At the raw spectra in Fig. 1(c), such valence subbands appear as small peaks. We note that the subbands exist not only at the inversion layer but also at the depletion layer in the space-charge layer region. The topmost valence

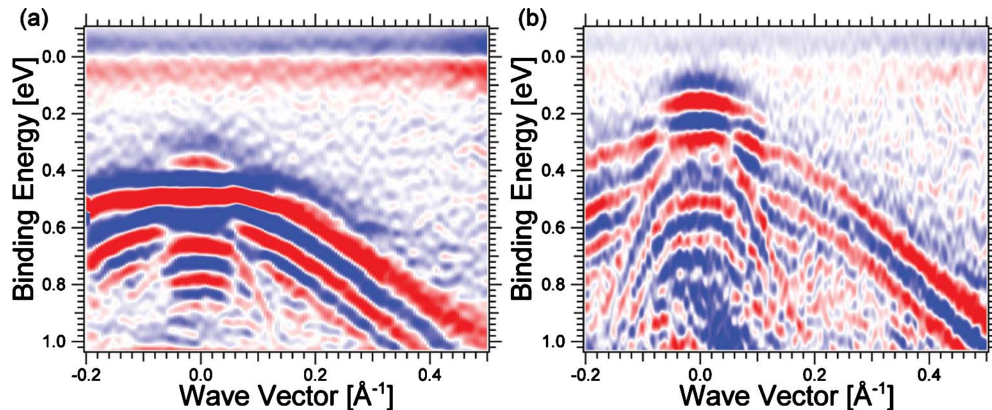

FIG. 3. (Color online) Valence-subband dispersions of (a) In- and (b) Pb-induced Si(111) ILs. The second derivative was applied in the energy direction to the raw ARPES intensity map for clarity. Wave vectors are along $[11\bar{2}]$. The red region corresponds to higher photoelectron intensity. Horizontal axes are converted from the photoelectron emission angle in raw data to the wave number.

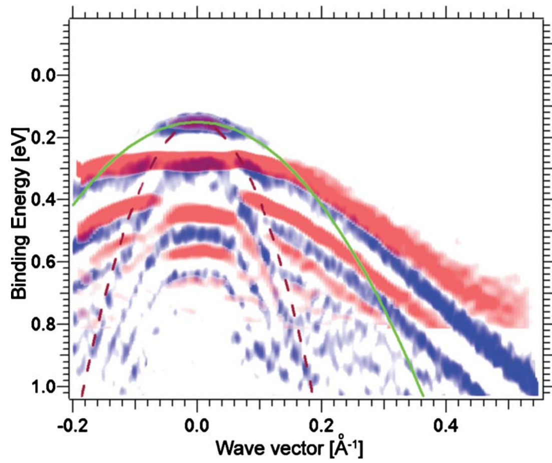

FIG. 4. (Color online) Comparison of the subbands formed in the two inversion layers IL(In) (red) and IL(Pb) (blue). The subband structure in IL(In) is shifted by 0.24 eV to the Fermi level to fit its ground subband to the subbands in IL(Pb). The solid and dashed lines are parabolic curves which correspond to effective masses $m^*_{11\bar{2}}(\text{hh})(0.57m_0)$ and $m^*_{11\bar{2}}(\text{lh})(0.15m_0)$.

subband in IL(Pb) is placed closer to the Fermi level by 0.24 eV than IL(In). This amount is approximately the same as the shift of the band bending (0.25 eV) shown in Fig. 2. The heavy and light in-plane mass subbands are crossing/repulsing at around $|k| \simeq 0.1$ Å^{-1}. The energy separations between the subbands depend on k at $|k| \leq 0.1$ Å^{-1}. This indicates that the subband shapes are modified due to interactions between the adjacent bands. In the outer region, $|k| > 0.1$ Å^{-1}, the energy separations are almost constant. In Fig. 4, the dispersion structures of the subbands in both ILs are displayed in the same frame to illustrate the influence of the amount of the band bending, namely, the surface carrier concentration on the subband structure. For comparison, subbands from IL(In) are shifted by 0.24 eV toward the Fermi level. It is seen that the energy separations of the adjacent subbands are larger in IL(Pb). This corresponds to the narrower width of IL(Pb) compared with IL(In). Further discussion on the energy separation will be given later. The curvatures of the subbands of the ILs are approximately the same with the exception of two points. One discrepancy exists in the second subband at $k=0.0$ Å^{-1}. The second subband of IL(Pb) at $k=0.0$ Å^{-1} is connected to the subband with light in-plane mass while the second subband of IL(In) at $k=0.0$ Å^{-1} is apparently connected to the subband with the heavy in-plane mass. This feature was observed over repeated experiments. This is explained by the difference of the band repulsion points of subbands of both ILs arising from the difference in the subband energy separations. The second discrepancy is at the highest heavy subband at $k \geq 0.3$ Å^{-1}. It is clear that in this region, the subband dispersion of IL(In) is flatter than that of IL(Pb). In the case of IL(In) surface, there is a surface-state band which crosses the Fermi level at 0.5 Å^{-1} and disperses toward the higher wave vector under the Fermi level.[54] The first heavy subband may interact with this surface state because both bands are close in E-k map and also close in real space. Other than the above two points, the dispersion curvatures look to be the same in both ILs.

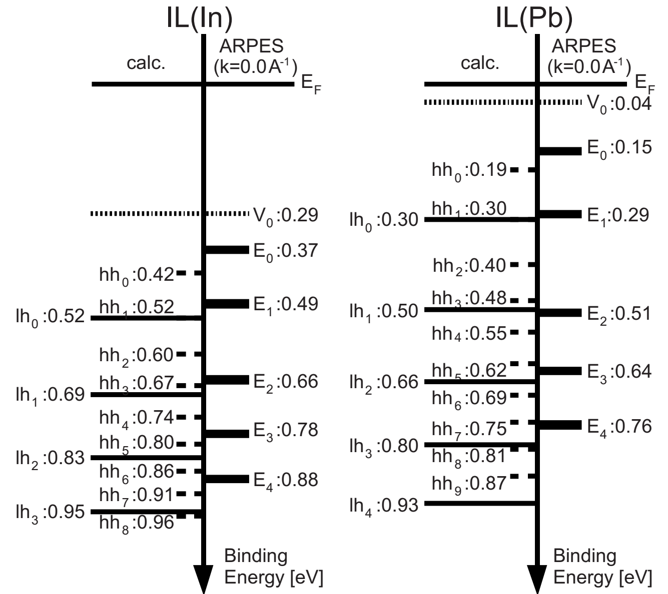

FIG. 5. Subband levels obtained by the calculation (left sides) and the ARPES (right sides) for IL(In) and IL(Pb). lh$_n$ and hh$_n$ are the levels belonging $m^*_z(\text{lh})$ and $m^*_z(\text{hh})$, respectively. Energy values by ARPES are employed from $k=0.0$ Å^{-1}.

It is interesting to compare this subband structure to the Si bulk valence band. Employing the $k \cdot p$ approximation and using the band parameters for Si,[55,56] the effective masses for bulk Si in $[11\bar{2}]$ direction are calculated to be $m^*_{11\bar{2}}(\text{hh}) = 0.57m_0$ and $m^*_{11\bar{2}}(\text{lh}) = 0.15m_0$. Here, hh and lh means heavy hole and light hole, respectively. The lines shown in Fig. 4 are parabolic curves with the above effective masses. The curvature of the parabolic line of $m^*_{11\bar{2}}(\text{hh})$ fits well with the experimental dispersion curve at $k < 0.12$ Å^{-1}. Because the valence-band parameters are derived for the small wave-vector region satisfying $\hbar^2k^2/2m\Delta \ll 1$, which corresponds to $k \ll 0.11$ Å^{-1} using spin-orbit splitting $\Delta = 0.044$ eV for Si, it is concluded that the effective mass of the top heavy valence subband has the effective mass of the bulk valence band within the above k region. Although there is a faint trace of the subband with light in-plane mass belonging to the fundamental subband level [Fig. 3(b)], it is not obvious whether the light-hole subband also has bulk effective mass $m^*_{11\bar{2}}(\text{lh})$ or not. The (in-plane) light-hole subbands belonging to higher indices were found to have effective masses slightly heavier than the bulk $m^*_{11\bar{2}}(\text{lh})$.

The relationship between the surface carrier concentration n_s and the effective mass of the Si(111) valence subband has been investigated by CR,[10] SdH,[4,57] and calculations.[26,27,58] The results of those studies are summarized in Refs. 10 and 35. The results are separated into two groups in terms of the value of the effective mass on n_s. The effective mass of one group[4,10,26,27] is around $0.5m_0$ and that of the other group[57,58] is around m_0 at $n_s = 3 \times 10^{12}$ cm^{-2}. These observed masses are believed to be a heavy-hole mass.[3] Although the reported CR mass and SdH mass are the averaged mass over all directions on the surface, the anisotropy of the valence sub-

TABLE I. Relation between the lh and hh masses in z ([111]) and x([11$\bar{2}$]) directions.

		z direction ([111])	
		lh	hh
x direction ([11$\bar{2}$])	lh		p_x
	hh	p_z	p_y

band is not so large in the case of Si(111) (Ref. 26) so the CR and SdH masses should be similar to the ARPES effective mass. Thus, our result supports the value of the former group. The value of latter group may correspond to the lower part of the subband structure, where the effective mass is obviously heavier as is clearly seen in Fig. 4.

All the early results indicate that the effective mass of the valence subband increases with n_s. In the case of the former group, the effective mass at $n_s=4\times 10^{12}$ cm^{-2} was obtained to be around $0.55m_0$–$0.6m_0$, which corresponds to the increase of 10–20 % from the value at $n_s=3\times 10^{12}$ cm^{-2}. This increase is attributed to an effect of electron-eletcron interaction. In contrast to the early results, the result obtained in this study indicates that the dispersion structure of the valence subband is not influenced by n_s at this range. Since data here is obtained at room temperature, unlike the early results by CR and SdH taken at low temperature, strong effect by electron-electron interaction cannot be expected. We can conclude from our data here that effective mass of the subband is constant at this n_s range at RT.

In Fig. 5, the valence-subband levels at $k=0.0$ Å^{-1} are compared to the values calculated by the triangular approximation (TA).[59] In the TA, the energy levels are expressed as $E_{m_z,n}=1/(2m_z)^{1/3}(\hbar eE_s)^{2/3}\gamma_n$, where γ_n is the Airy function and $\gamma_0=2.338$, $\gamma_1=4.088$, $\gamma_2=5.521$, $\gamma_3=6.787$, and for higher n, $\gamma_n\simeq[\frac{3\pi}{2}(n+\frac{3}{4})]^{2/3}$.[60] E_s is the electric field at the surface. m_z is the effective mass of Si in z ([111]) direction. It is obvious from this equation that the energy levels are classified into two groups according to whether the corresponding m_z is heavy or light. The masses are calculated to be $m_z^*(\text{hh})=0.72m_0$ and $m_z^*(\text{lh})=0.14m_0$ using the valence-band parameters for Si.[55,56] The relationships between the orbital type and the effective mass in z and x directions are shown in Table I. For example, the bands which have heavy mass in z direction are composed of p_x and p_y orbitals and their masses in x direction are light and heavy, respectively. The calculated energy levels are labeled as lh$_n$ and hh$_n$ according to n and the type of m_z which they belong to. From the comparison between the observed and calculated levels of In(Pb) shown in Fig. 5, it is found that the observed levels E_1 to E_4 are close to the calculated levels lh$_0$ to lh$_3$ within 0.04 eV. As an interpretation of this, we speculate that the observed levels are those which have $m_z^*(\text{lh})$, and that the ARPES intensity of the levels belonging to $m_z^*(\text{hh})$ are weak at $k=0.0$ Å^{-1}. The sharp ARPES peaks in the spectrum shown in Fig. 1 indicate that the observed levels are not superposition of both lh and hh levels having comparable ARPES intensities. In the case of IL(In), the discrepancies between them are larger particularly for E_4 and lh$_3$ (0.07 eV) However, because the energy differences between the neighboring measured levels are close to the calculated levels for $m_z^*(\text{lh})$, the above interpretation is still valid. The observed level E_0 should then correspond to hh$_0$ although the discrepancies are large in both ILs. To explain this ARPES intensity difference, effects from the matrix element of photoemission process and/or effects of surface states on the reflection at the surface are currently being considered and will be published in the future. In this paper, only a simplified triangular approximation is used to calculate the subband energy levels. Further theoretical calculations using more realistic models are needed to discuss the complicated subbands dispersion structures and their energy levels around Γ point.

The deepest subband at $k=0.0$ Å^{-1} detected in this study lies at 0.88 eV in IL(In) and at 0.76 eV in IL(Pb). At these energies, the spatial extension of the subband wave function in z direction is large due to the triangularlike shape of the confinement potential. The spatial extension of the subband wave function can be deduced from the band-bending curvature in Fig. 2. The spatial extensions of the deepest subbands in the above binding energies are obtained to be 15 nm in both ILs from Fig. 2. According to Ref. 61, the hole mobility of Si with the dopant concentration of 10^{18} cm^{-3} is 1.5×10^2 cm^2/V s at room temperature. The mean-free path of the hole is calculated to be 4 nm using this mobility. Thus, the spatial extension of the deepest subbands is longer than the mean-free path by a factor of 4. In such a case, the scattering would disturb the coherency and the formation of the wave function extending in z direction. In ARPES spectra, this makes the subband peak weak and broad. Consequently, it is concluded that the subband extending more than 15 nm was not detected in this study. This suggests that a narrow IL is necessary to observe the subband dispersion by ARPES.

In conclusion, we investigated the dispersion structures of the hole subbands in Si(111) p-type ILs with different surface carrier concentration directly by ARPES. By changing the IL shape, the top valence-subband level shifted according to the shift of the confining potential height. The measured energy levels other than $n=0$ were in good agreement with that of the valence subbands calculated by the TA with the bulk light-hole mass $m_z^*(\text{lh})$. The observed ground ($n=0$) levels were attributed to the calculated levels with the bulk heavy-hole mass $m_z^*(\text{hh})$. The effective masses of the subbands were similar to the bulk hole masses and not modified by the change in surface carrier concentration used in this study.

This work was supported by JST-CREST, Nippon Sheet Glass Foundation for Materials Science and Engineering, and Semiconductor Technology Academic Research Center (STARC).

*sakura@ms.naist.jp

[1] J. R. Schrieffer, in *Semiconductor Surface Physics*, edited by R. H. Kingston (University of Pennsylvania Press, Philadelphia, 1957), p. 55.
[2] A. B. Fowler, F. F. Fang, W. E. Howard, and P. J. Stiles, Phys. Rev. Lett. **16**, 901 (1966).
[3] K. von Klitzing, G. Landwehr, and G. Dorda, Solid State Commun. **14**, 387 (1974).
[4] K. von Klitzing, G. Landwehr, and G. Dorda, Solid State Commun. **15**, 489 (1974).
[5] J. L. Smith and P. J. Stiles, Phys. Rev. Lett. **29**, 102 (1972).
[6] K. von Klitzing, G. Landwehr, and G. Dorda, Proceedings of the 2nd International Conference on Solid Surfaces, 1974 [Jpn. J. Appl. Phys. Suppl. **2**, Pt. 2, 351 (1974)].
[7] S. James Allen, Jr., D. C. Tsui, and J. V. Dalton, Phys. Rev. Lett. **32**, 107 (1974).
[8] G. Abstreiter, J. F. Koch, P. Goy, and Y. Couder, Phys. Rev. B **14**, 2494 (1976).
[9] H. Küblbeck and J. P. Kotthaus, Phys. Rev. Lett. **35**, 1019 (1975).
[10] J. P. Kotthaus and R. Ranvaud, Phys. Rev. B **15**, 5758 (1977).
[11] R. J. Wagner, T. A. Kennedy, B. D. McCombe, and D. C. Tsui, Phys. Rev. B **22**, 945 (1980).
[12] G. Abstreiter, P. Kneschaurek, J. P. Kotthaus, and J. F. Koch, Phys. Rev. Lett. **32**, 104 (1974).
[13] T. A. Kennedy, R. J. Wagner, B. D. McCombe, and D. C. Tsui, Phys. Rev. Lett. **35**, 1031 (1975).
[14] A. Kamgar, P. Kneschaurek, G. Dorda, and J. F. Koch, Phys. Rev. Lett. **32**, 1251 (1974).
[15] P. Kneschaurek, A. Kamger, and J. F. Koch, Phys. Rev. B **14**, 1610 (1976).
[16] A. D. Wieck, E. Batke, D. Heitmann, J. P. Kotthaus, and E. Bangert, Phys. Rev. Lett. **53**, 493 (1984).
[17] A. D. Wieck, E. Batke, D. Heitmann, and J. P. Kotthaus, Phys. Rev. B **30**, 4653 (1984).
[18] F. Martelli, C. Mazuré, and F. Koch, Phys. Rev. B **30**, 6023 (1984).
[19] G. Abstreiter, U. Claessen, and G. Tränkle, Solid State Commun. **44**, 673 (1982).
[20] M. Baumgartner, G. Abstreiter, and E. Bangert, J. Phys. C **17**, 1617 (1984).
[21] F. Neppl, J. P. Kotthaus, J. F. Koch, and Y. Shiraki, Phys. Rev. B **16**, 1519 (1977).
[22] F. Neppl, J. P. Kotthaus, and J. F. Koch, Phys. Rev. B **19**, 5240 (1979).
[23] E. Gornik and D. C. Tsui, Phys. Rev. Lett. **37**, 1425 (1976).
[24] T. K. Lee, C. S. Ting, and J. J. Quinn, Solid State Commun. **16**, 1309 (1975).
[25] F. J. Ohkawa, Surf. Sci. **58**, 326 (1976).
[26] F. J. Ohkawa and Y. Uemura, Prog. Theor. Phys. **57**, 164 (1975).
[27] E. Bangert, K. von Klitzing, and G. Landwehr, in *Proceedings of the 12th International Conference on the Physics of Semiconductors*, Stuttgart, 1974, edited by M. H. Pilkuhn (Teubner, Stuttgart, 1974), p. 714.
[28] B. Vinter, Phys. Rev. Lett. **35**, 598 (1975).
[29] B. Vinter, Phys. Rev. Lett. **35**, 1044 (1975).
[30] T. Ando, Phys. Rev. B **13**, 3468 (1976).
[31] F. J. Ohkawa, J. Phys. Soc. Jpn. **41**, 122 (1976).
[32] B. Vinter, Phys. Rev. B **15**, 3947 (1977).
[33] S. Das Sarma and B. Vinter, Phys. Rev. B **28**, 3639 (1983).
[34] W. O. G. Schmitt, Phys. Rev. B **50**, 15221 (1994).
[35] T. Ando, A. B. Fowler, and F. Stern, Rev. Mod. Phys. **54**, 437 (1982).
[36] S. Rodríguez, J. A. López-Villanueva, I. Melchor, and J. E. Carceller, J. Appl. Phys. **86**, 438 (1999).
[37] S. Rodríguez, F. Gámiz, A. Palma, P. Cartujo, and J. E. Carceller, J. Appl. Phys. **88**, 1978 (2000).
[38] Y. T. Hou and M. F. Li, IEEE Trans. Electron Devices **48**, 1188 (2001).
[39] Y. T. Hou and M. F. Li, Jpn. J. Appl. Phys. **40**, L144 (2001).
[40] Y. T. Hou, M. F. Li, Y. Jin, and W. H. Lai, J. Appl. Phys. **91**, 258 (2002).
[41] M. V. Fischetti, Z. Ren, P. M. Solomon, M. Yang, and K. Rim, J. Appl. Phys. **94**, 1079 (2003).
[42] K. Natori, T. Shimizu, and T. Ikenobe, Jpn. J. Appl. Phys. **42**, 2063 (2003).
[43] S. Takagi, T. Mizuno, T. Tezuka, N. Sugiyama, S. Nakaharai, T. Numata, J. Koga, and K. Uchida, Solid-State Electron. **49**, 684 (2005).
[44] S. N. Takeda, N. Higashi, and H. Daimon, Phys. Rev. Lett. **94**, 037401 (2005).
[45] J. Kraft, S. L. Surnev, and F. P. Netzer, Surf. Sci. **340**, 36 (1995).
[46] S. Takeda, X. Tong, S. Ino, and S. Hasegawa, Surf. Sci. **415**, 264 (1998).
[47] H. H. Weitering, A. R. H. F. Ettema, and T. Hibma, Phys. Rev. B **45**, 9126 (1992).
[48] K. Horikoshi, X. Tong, T. Nagao, and S. Hasegawa, Phys. Rev. B **60**, 13287 (1999).
[49] V. G. Lifshits, A. A. Saranin, and A. V. Zotov, *Surface Phases on Silicon* (Wiley, Chichester, 1994).
[50] S. Hüfner, *Photoelectron Spectroscopy* (Springer, Berlin, 1996).
[51] W. Mönch, *Semiconductor Surfaces and Interfaces* (Springer, Berlin, 1995).
[52] F. J. Himpsel, G. Hollinger, and R. A. Pollak, Phys. Rev. B **28**, 7014 (1983).
[53] H. M. Zhang, K. Sakamoto, G. V. Hansson, and R. I. G. Uhrberg, Phys. Rev. B **78**, 035318 (2008).
[54] E. Rotenberg, H. Koh, K. Rossnagel, H. W. Yeom, J. Schafer, B. Krenzer, M. P. Rocha, and S. D. Kevan, Phys. Rev. Lett. **91**, 246404 (2003).
[55] C. Kittel, *Introduction to Solid State Physics* (Wiley, New York, 1986).
[56] C. Kittel, *Quantum Theory of Solids* (Wiley, New York, 1987).
[57] A. A. Lakhani, P. J. Stiles, and Y. C. Cheng, Phys. Rev. Lett. **32**, 1003 (1974).
[58] L. M. Falicov and N. Garcia, Solid State Commun. **17**, 473 (1975).
[59] F. Stern, Phys. Rev. B **5**, 4891 (1972).
[60] M. Abramowitz and I. A. Stegun, *Handbook of Mathematical Functions* (Dover, New York, 1972).
[61] S. M. Sze and K. K. Ng, *Physics of Semiconductor Devices* (Wiley, New Jersey, 2007).